Mechanism and Machine Theory 185 (2023) 105311

Contents lists available at ScienceDirect

Mechanism and Machine Theory

journal homepage: www.elsevier.com/locate/mechmt

Research paper

Kinematic Analysis of three degrees of freedom planar parallel continuum mechanisms

Oscar Altuzarra *, Mónica Urizar, Massimo Cichella, Víctor Petuya

Department of Mechanical Engineering, University of the Basque Country UPV/EHU, Bilbao, Spain

ARTICLE INFO

Keywords:
Parallel continuum mechanism
Kirchhoff rod
Kinematics
Deformation modes
Instability

ABSTRACT

Parallel continuum mechanisms are a type of compliant mechanisms comprising a rigid end-effector connected to a fixed frame by flexible and slender elements in a closed-kinematic morphology, being their flexibility the source of mobility. Solving the position problem involves the static equilibrium of the whole device considering the nonlinear large deformations of slender elements. Numerical iterative solutions are already available to solve real-time simulations. However, an assembled solution, which meets both geometric conditions and static equilibrium, is needed to start the process. A comprehensive Kinematic Analysis in the classical sense is not fully established yet. The aim of the paper is to propose a procedure that solves the full inverse and forward kinematic problems for planar three degrees of freedom systems, hence obtaining the multiple solutions arising from the closed-loop structure and the multiplicity of the deformation mode of slender links. From those solutions, finding of the different aspects that comprise the workspace is possible, as well as determining singularities and instability loci.

1. Introduction

Parallel Continuum Mechanisms (PCMs) are flexible mechanical devices with a rigid end-effector that is connected to a fixed frame using flexible slender links whose deformation is the cause of its mobility [1]. These are derived from continuum mechanisms, where parallel assemblies of tendons, rigid parts, and flexible backbones are common ways of generating slender systems motivated by the problem of manipulation in confined, hard to reach workspaces [2], and suitable for minimally invasive procedures due to their dexterity and ease of miniaturization [3]. Aforementioned mechanisms belong to the group of Compliant mechanisms, those that acquire mobility thanks to the relative flexibility of some of their parts [4,5].

Kinematic Analysis of PCMs aims to solve position problems, define singularities, obtain those aspects that build up workspaces, and evaluate instability poses. The latter is a distinctive property of flexible mechanisms, i.e. as force equilibrium involves flexible elements, such equilibrium poses should be stable for the mechanism to withstand a certain motion under given load [6].

Regarding position problems in PCMs of slender elements, an appropriate model for the nonlinear deformation of the rods used as elements is needed. Pseudo-rigid-body model (PRBM) method [4,7] is the simplest approach but has important limitations because it does not allow changes of deformation mode (commonly known in the literature as buckling mode), which are common along any path in most systems. Another group of kinetostatic modelling methods are of the type of discretization-based approaches that use structural compliance matrices to model each discretized element that build up an equivalent mechanism [8–10]. A consequent natural step in the field of discretization approaches is the use of Finite Element models [11], which can be implemented for precise, ad hoc analysis of nearly final designs, but are of more limited use in early stages of design. Regarding continuous models, Cosserat

* Corresponding author.
E-mail address: oscar.altuzarra@ehu.eus (O. Altuzarra).

https://doi.org/10.1016/j.mechmachtheory.2023.105311
Received 11 October 2022; Received in revised form 20 February 2023; Accepted 20 February 2023
Available online 7 March 2023

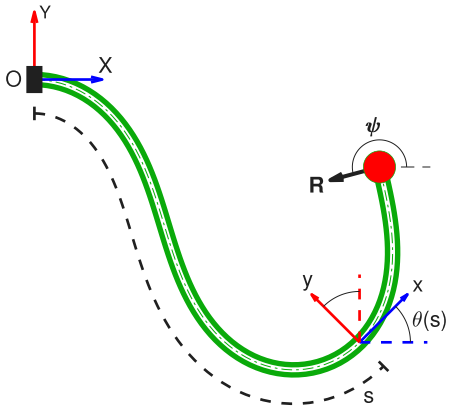

Fig. 1. Deformed shape of a clamped-free rod under load R at end-tip.

rod model [12] is used extensively in modelling systems with rods subjected to large nonlinear deformations. This model can be mathematically expressed in different ways, with a nonlinear system of differential equations (ODEs) the most accurate one. The closed-loop system of flexible rods and rigid elements generates a coupling of large deformation modelling equations and force equilibrium ones to accommodate the deformation's internal forces and moments to the load. Based on this approach, a sustained line of research on hexapod-like flexible devices has been performed, solving a variety of problems such as real-time position control and elastic analysis [13–16] and dynamics [17,18]. The main drawback is that, to start the analysis, it requires a known pose, so that close positions can be solved using a direct integration of the system of ODEs from previous values of state parameters. This is plausible for path analysis, but it does not allow for the solving of the multiplicity of solutions, and hence a comprehensive Kinematic Analysis.

Planar PCMs considered here have slender elements that are straight rods in their free-stress reference configuration; they are usually subjected to planar Dynamics conditions, i.e. force loads are on the plane and applied moments are perpendicular to the plane; and therefore, rods can be considered to be subjected to neither shear nor extension. Also, the material constitutive law used is linear. Under such circumstances, the Cosserat nonlinear differential system of equations leads to a simplified model called the Kirchhoff rod model. The key point of such model is that the resultant system of differential equations can be manipulated to allow an analytical integration through elliptic integrals functions, a technique widely used in the field of continuum robots and manipulators [19]. Moreover, each deformed shape of a rod is univocally defined by the deformation mode (d-mode), and two parameters (k and ψ) whose space is enclosed in a certain range of real values [4]. Hence, when looking for the solution of the position problem of these mechanisms the objective will be to get those sets of parameters for the flexible rods of the system such that equilibrium of the whole exists. As the space of those parameters is limited, it is possible to search for all multiple solutions even without an initial given pose. Authors presented a procedure to solve such problem in planar mechanisms of 2 degrees of freedom (DoF) with punctual end-effector in [20] using numerical optimization. Later, we presented a certified solution method – interval analysis – [21] to solve the same problem, demonstrating the feasibility to perform comprehensive Kinematic Analysis on such closed-loop flexible mechanisms. Our recent research efforts have been focused on finding efficient ways to get such solutions so that Kinematic analysis equivalent to those performed in rigid-link devices can be carried out [22,23]. Now, we are extending these approaches to: more complex PCMs with other actuation systems and additional degrees of freedom, including singularity and instability evaluation, and aiming to analogous Kinematic Analysis to those performed in classical Parallel Kinematics.

The paper is organized as follows: Section 2 is a short review of Kirchhoff rod model in planar systems solved using elliptic integrals [4,24]; Section 3 contains the definition of the type of mechanisms analysed; Sections 4 and 5 present the procedures to get all multiple solutions of the Inverse and Direct position problems; Section 6 recalls the use of iterative position analysis in conjunction with singularity analysis and instability analysis to get all aspects of the workspace performing a classical Kinematic Analysis; and Section 7 discuss the experimental application of these results. Finally, in Section 8, the conclusions of this paper are drawn.

2. Fundamentals of Kirchhoff rod model

In this section, the reader will find a summary of the fundamentals on approaching the nonlinear analysis of the deformation of elastic planar rods with the elliptic integrals method that are treated in detail in [4,12]. As planar kinematics is considered, no out of plane action is considered, and then no out of plane bending or torsion applies. The following two mathematical structures define the shape of a deformed planar rod: a parametric Cartesian curve, $\mathbf{p}(s) \in \mathbb{R}^2$, identifying the centroid coordinates x and y of each cross-section, and the angle $\theta(s)$ which establishes the orientation of a local frame attached to the cross-section, as shown in Fig. 1. Position $\mathbf{p}(s)$ and orientation $\theta(s)$ depend on the scalar reference arc-length s defined over a finite interval, $s \in [0, L]$, where L is the length of the rod.

The position and orientation of each part of the rod evolve along the arc length according to rates of change, linear $\mathbf{v}(s) \in \mathbb{R}^2$ and angular $\mathbf{u}(s) \in \mathbb{R}$. These rates of change are defined in the local frame, and related to the derivatives of position $\mathbf{p}(s)$ and orientation $\theta(s)$ with respect to s as:

$$\begin{Bmatrix} \frac{dx}{ds} \\ \frac{dy}{ds} \\ \frac{d\theta}{ds} \end{Bmatrix} = \begin{Bmatrix} v_x \cos(\theta) - v_y \sin(\theta) \\ v_x \sin(\theta) + v_y \cos(\theta) \\ u_z \end{Bmatrix} \tag{1}$$

Linear $\mathbf{v}(s)$ and angular $\mathbf{u}(s)$ rates of change are also related to internal forces $\mathbf{n}(s)$ [N] and moments $\mathbf{m}(s)$ [Nm] (defined in a fixed frame) through the material constitutive equations $\mathbf{v} = \mathbf{K}_{SE}^{-1}\mathbf{R}^T\mathbf{n} + \mathbf{v}_\circ$ and $\mathbf{u} = \mathbf{K}_B^{-1}\mathbf{R}^T\mathbf{m} + \mathbf{u}_\circ$, where $\mathbf{K}_{SE}$ and $\mathbf{K}_B$ are stiffness matrices for shear–extension and bending respectively, where for initially straight rods $\mathbf{v}_\circ = [1\ 0\ 0]^T$ and $\mathbf{u}_\circ = \mathbf{0}$, and where $\mathbf{R}$ is the rotation matrix that transforms magnitudes between a fixed frame and the local frame. For linear constitutive material law, stiffness matrices are diagonal and, hence, we get

$$v_x = \frac{1}{EA}\left[n_x \cos(\theta) + n_y \sin(\theta)\right] + 1 \tag{2}$$

$$v_y = \frac{1}{GA}\left[-n_x \sin(\theta) + n_y \cos(\theta)\right] \tag{3}$$

$$u_z = \frac{m_z}{EI} \tag{4}$$

where E is the elastic modulus, A the cross section area, G the shear modulus, and I the cross section's area moment of inertia. Note that some materials may require more complex material laws.

The simplified model of deformation, known as Kirchhoff rod model, is used. Rod's shear and extension are neglected because for slender rods the relative magnitude of internal forces to stiffness justifies the approximation of $v_x = 1$ and $v_y = 0$ and then the deformed shape is considered to be caused only by bending, namely

$$\begin{Bmatrix} \frac{dx}{ds} \\ \frac{dy}{ds} \\ \frac{d\theta}{ds} \end{Bmatrix} = \begin{Bmatrix} \cos\theta \\ \sin\theta \\ \frac{m_z}{EI} \end{Bmatrix} \tag{5}$$

To establish the equilibrium of forces and moments for every portion of the deformed rod, we consider an infinitesimal piece of the rod between sections located at s and $s + ds$. Equilibrium nonlinear differential equations describing the evolution of the internal force $\mathbf{n}(s)$ and moment $\mathbf{m}(s)$ along rod's arc length, subjected to distributed forces per arc length $\mathbf{f}(s)$ [N/m] and moments $\mathbf{l}(s)$ [Nm/m] applied on the rod, arises:

$$\begin{aligned} \frac{d\mathbf{n}(s)}{ds} + \mathbf{f}(s) &= \mathbf{0} \\ \frac{d\mathbf{m}(s)}{ds} + \frac{d\mathbf{p}(s)}{ds} \times \mathbf{n}(s) + \mathbf{l}(s) &= \mathbf{0} \end{aligned} \tag{6}$$

If neither $\mathbf{f}$ nor $\mathbf{l}$ is applied, we get the following components of Eq. (6):

$$\begin{Bmatrix} \frac{dn_x}{ds} \\ \frac{dn_y}{ds} \\ \frac{dm_z}{ds} \end{Bmatrix} = \begin{Bmatrix} 0 \\ 0 \\ n_x \sin\theta - n_y \cos\theta \end{Bmatrix} \tag{7}$$

This results in a constant internal force $\mathbf{n}$. If only end-point load is applied (R and ψ being its magnitude and orientation, respectively, as depicted in Fig. 1), for constant E and I, assuming a stress-free reference straight rod, considering the last row in Eq. (5), and upon substitution into Eq. (7), we get a single ODE in θ:

$$\frac{d^2\theta}{ds^2} = \frac{1}{EI}\left(R\cos\psi\sin\theta - R\sin\psi\cos\theta\right) = \frac{R}{EI}\sin(\theta - \psi) \tag{8}$$

Integration of Eq. (8), by making use of some change of variables [24], yields:

$$\sqrt{R} = \frac{\sqrt{EI}}{L}\left[F(k,\phi_2) - F(k,\phi_1)\right] \tag{9}$$

where $F(k,\phi)$ is the incomplete elliptic integral of the first kind, k is a constant $k \in [-1,1]$, whereas ϕ is a transformed variable running continuously along the rod as s and θ do. Angle ϕ varies between extremes ϕ_1 and ϕ_2, which are defined by the boundary conditions of the rod. For example, let us consider a rod clamped horizontally at the first extreme whereas the other end is free, as represented in Fig. 1. Then, on the one hand, ϕ_1 is

$$\phi_1 = \arcsin\left(\frac{1}{k}\cos\left(\frac{\psi}{2}\right)\right) \tag{10}$$

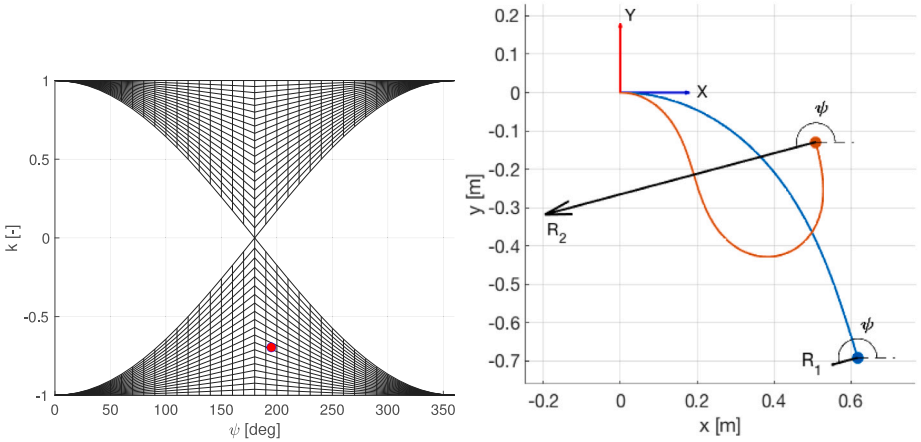

(a) Parameter Space (k, ψ) and chosen duple (b) Rod shape for buckling modes 1 and 2

Fig. 2. Parametric definition of a planar flexible rod.

while on the other end there is an inflection point of the curve, because m_z and so $\frac{d\theta}{ds}$ is null, yielding ϕ_2

$$\phi_2 = (2q-1)\pi/2 \quad \text{for } q = 1, 2, \ldots \tag{11}$$

where q identifies the so-called d-mode (also known as buckling mode). Each d-mode q has a q number of inflection points, i.e., mode 1 has one inflection point (precisely at the free end), mode 2 has two, and so on.

Upon integration of Eq. (5), we can obtain now coordinates x and y of points on the rod along the arc length corresponding to parameter ϕ_i, defining the deformed shape of the rod:

$$\begin{aligned} x(\phi_i) = &- \sqrt{\frac{EI}{R}} \cos\psi \left[2E(k,\phi_i) - 2E(k,\phi_1) - F(k,\phi_i) + F(k,\phi_1)\right] \\ &- \sqrt{\frac{EI}{R}} 2k \sin\psi \left[\cos\phi_i - \cos\phi_1\right] \end{aligned} \tag{12}$$

$$\begin{aligned} y(\phi_i) = &- \sqrt{\frac{EI}{R}} \sin\psi \left[2E(k,\phi_i) - 2E(k,\phi_1) - F(k,\phi_i) + F(k,\phi_1)\right] \\ &+ \sqrt{\frac{EI}{R}} 2k \cos\psi \left[\cos\phi_i - \cos\phi_1\right] \end{aligned} \tag{13}$$

where $E(k, \phi)$ is the incomplete elliptic integral of the second kind.

Hence, both Eqs. (5) and (7) have been integrated to yield Eqs. (9), (12), and (13), i.e., a parametric system that uniquely defines a deformed rod in terms of k and ψ parameters, for known boundary conditions and a certain d-mode q. Note that feasible values of k depend on parameter ψ, so that ϕ_1, in Eq. (10), is real, i.e. between $|k_{min}| = \cos\psi/2$ and $|k| = 1$. This condition restricts the parameter space (k, ψ) for these boundary conditions as shown in Fig. 2(a). As it can be seen in Fig. 2, if a duple of values k and ψ inside the feasible range is selected, Fig. 2(a), we will univocally get the deformed shape of the rod for each d-mode desired, as depicted in Fig. 2(b) for d-modes 1 and 2.

The aforementioned parametrization, allowed by this Kirchhoff planar deformation model integrable using elliptic integrals, is of capital importance in the following procedures because solutions to the position problems of flexible mechanisms will be defined by a limited number of parameters (k^i, ψ^i per rod i) whose possible values are in a closed space.

3. Mechanisms under study

The planar parallel continuum mechanisms considered in this work are 3 degrees of freedom (DoF) fully parallel mechanisms formed by closed-loop assemblies of three flexible rods connected to a rigid-body moving platform. The end-effector's moving frame ($\mathcal{P}$, xyz) is located at reference point $\mathcal{P}$ which corresponds to the centroid of the triangular platform $B_1B_2B_3$. Flexible rods' end-tips are attached to the moving frame at points B_i via revolute joints. Flexible rods are connected to the fixed element and actuated in three different ways described below. A fixed reference system ($\mathcal{O}$, XYZ) is defined on the fixed element.

In Fig. 3, the three types of PCMs under study are represented. The three different types of attachment and actuation of the flexible rods chosen are the most feasible ones. The following notation is used to define each mechanism: the underline identifies the actuated variable, P corresponding to a prismatic joint, F denotes the flexible rod (only bending about an axis perpendicular to the plane) and R the revolute joint.

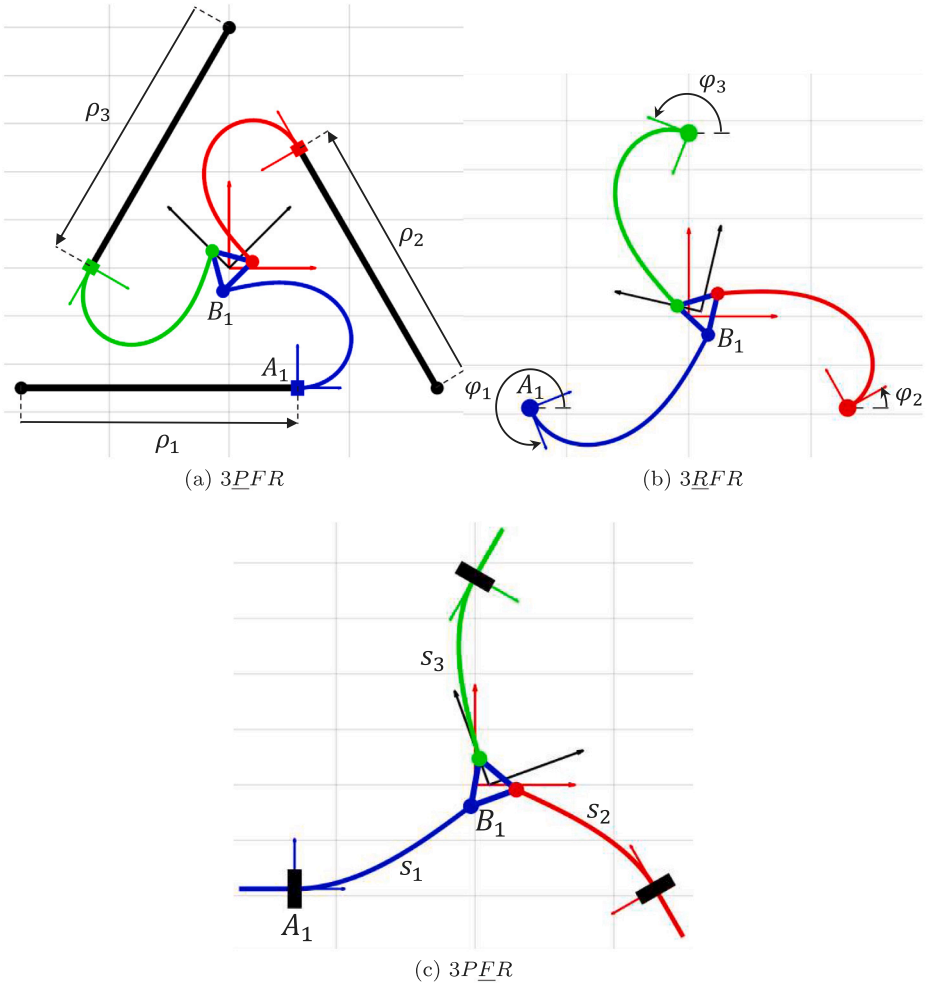

(a) $3\underline{P}FR$ (b) $3\underline{R}FR$

(c) $3P\underline{F}R$

Fig. 3. PCMs of 3 DoF.

Fig. 3(a) shows the $3\underline{P}FR$ mechanism, where each rod is actuated by a prismatic slider, the flexible rod has a constant length L connecting to the platform with a revolute joint. Flexible rod's first-tip A_i (subscript i identifies the rod) is clamped to an actuated linear table of fixed direction. A local frame $(\mathcal{A}_i, x_i y_i)$ is attached to the clamping, x_i axis oriented with the clamped slope. Distance to point A_i on the actuated prismatic joint from a fixed reference point O_i on the linear guide defines input length ρ_i.

Fig. 3(b) represents the $3\underline{R}FR$ mechanism, each rod of length L being actuated by a revolute joint. Flexible rod's first-tip A_i is clamped to the actuated revolute joint. A local frame $(\mathcal{A}_i, x_i y_i)$ is attached to the clamping, x_i axis being oriented with the clamped slope, and such rotating axis defines the input angle ϕ_i with reference to fixed frame's X axis.

Finally, in Fig. 3(c) the $3P\underline{F}R$ mechanism is shown, where the length of the flexible rod is not constant and indeed it corresponds to the actuated variable s_i. Flexible rods slide through a fixed prismatic pair at A_i. A local frame $(\mathcal{A}_i, x_i y_i)$ is attached to the prismatic pair, x_i axis oriented with the slope of sliding. Length of the rod free to bend from A_i to B_i, s_i, is the input variable of the mechanism.

With above definitions, all flexible rods have the same boundary conditions as in Fig. 1, with coordinates defined in the corresponding local frames $(\mathcal{A}_i, x_i y_i)$ given by Eqs. (12) and (13). Based on the fundamentals described in Section 2, flexible rods i are ruled by Eqs. (12), (13) and (9), and uniquely defined by parameters k^i and ψ^i, once a d-mode is chosen for them (see Fig. 2). The quasi-static position problem of the deformed mechanism is solved by finding the set of parameters k^i and ψ^i for each rod subject to the corresponding boundary conditions, hence six unknowns. Load applied at the end-effector is an input (3 parameters) alongside either the three input values at actuators for the Forward Kinematics (FK) problem, or the three pose parameters of the end-effector for the Inverse Kinematic (IK) problem.

The equivalent rigid parallel manipulators to these PCMs are shown in Fig. 4. For the flexible $3\underline{P}FR$, the rigid $3\underline{P}RR$ would perform comparable motions; the manipulator analogous to the $3\underline{R}FR$ would be the $3\underline{R}RR$; and finally, the $3P\underline{F}R$ shares similarities with the $3R\underline{P}R$.

It must be stressed that flexible PCMs behave kinematically in a more or less similar way to these equivalent rigid manipulators when rods' d-mode is 1, diverging dramatically as higher d-modes appear (which is not rare for d-mode 2 but requires a very

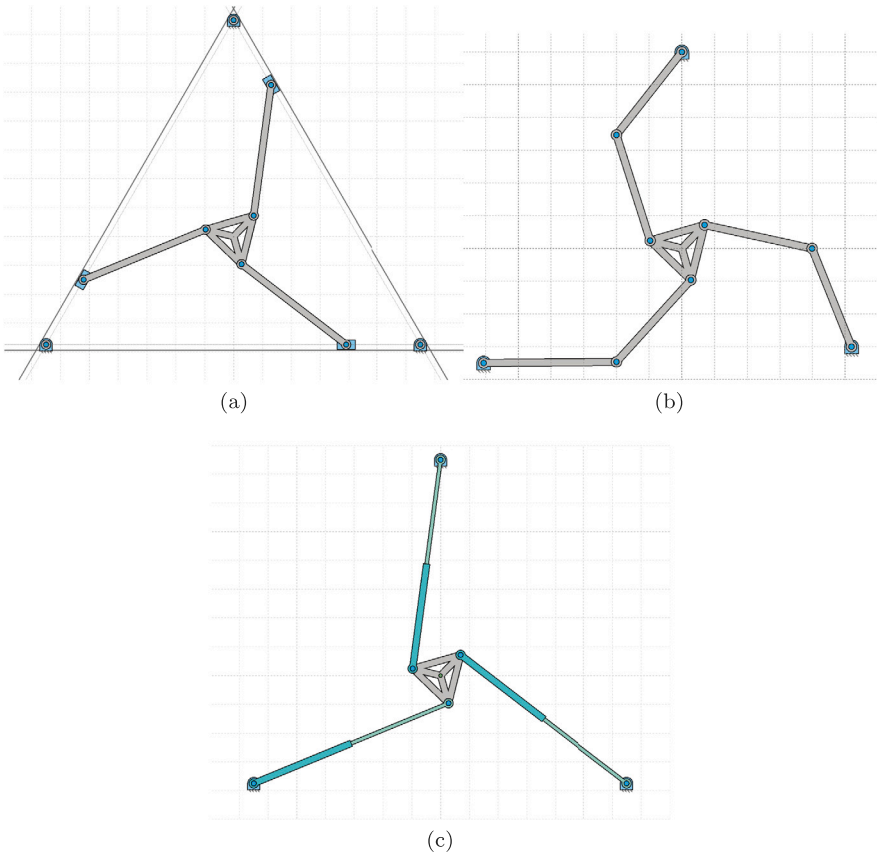

Fig. 4. Equivalent rigid manipulators: (a) $3\underline{P}RR$, (b) $3\underline{R}RR$ and (c) $3R\underline{P}R$.

high deformation energy and involves an important risk of self collisions for higher ones). Also, it must be noted that whereas the number of IK solutions, for the rigid manipulators, only depends on the geometric conditions that the legs must satisfy when the end effector is located at a certain pose, in the case of the flexible manipulators additional conditions given by the fulfilment of static equilibrium must be satisfied. Besides, the possibility of working in different buckling modes also affects the number of IK solutions. As a consequence, the use of pseudo rigid body models to analyse the full solution of position problems has a very limited success, and a more elaborated model is required.

4. Solving the full inverse kinematic problem

Solving the inverse kinematics problem (IK) implies obtaining the unknown input values of the actuators once the pose of the end effector is given (3 in-data). In addition, in these flexible mechanisms the load must be considered as an input to the problem (3 additional in-data), and the complete definition of the mechanism configuration (the deformed shape) is the objective to be solved. Obtaining the deformed shape of the flexible rods means getting the 6 parameters k^i and ψ^i. Out of these, actuators' values can be obtained geometrically defining the output of the IK problem. Additionally, a full inverse solution means obtaining all multiple solutions to a given end-effector's pose and load, these arising from the non linearity of closed-loop equations as well as from the multiple d-modes that a flexible rod may reach.

As mentioned, in flexible mechanisms, apart form the geometric conditions that have to be fulfilled, we have to stress that a force equilibrium must be reached between the load and forces generated in the deformation process. This double condition is exploited in the design of the proposed procedure.

The first step is to choose a certain d-mode for each flexible rod, this delimits the search procedure to those mechanism configurations with the corresponding d-modes chosen, e.g. commonly the first search will be with d-mode 1 for all rods. Other combinations of d-modes will be found by running the procedure with the new choice of d-modes bearing in mind that higher d-modes require higher energy levels and then are less feasible.

Second, the procedure will use some distinct geometric boundary conditions that can be derived for each of the leg types described in Section 3 to reduce the search in the parameter space. Such geometric conditions will be applied to determine a subset of possible solutions in the closed parameter space of all solutions k^i and ψ^i.

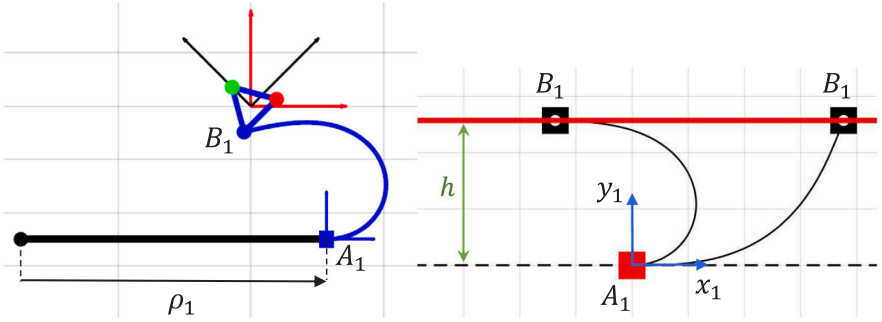

(a) In the fixed frame (b) In the local frame

Fig. 5. Geometric condition for leg type $\underline{P}FR$.

The third step is to check the conditions of static equilibrium on the latter subset of solutions fulfilling the geometric conditions, reducing them to a finite number of IK solutions.

Fourth, each of those solutions are then analysed to determine if they are regular solutions in a double sense. First, we check if they are stable equilibrium configurations of the flexible mechanism using a variational approach. And second, Kinematic Jacobians are obtained numerically to check closeness to singularity locus.

Finally, the resultant solutions have to be checked to verify if they are feasible with respect to other practical criteria. For example, they are to be checked for collision between rods or/and with the end-effector, rods' loop shapes, stress failure, and so on. Some of these effects can be detected using geometric functions inside a last verification part of the algorithm. In the following, we have left this last issue apart so that the full potential of the method can be appreciated showing all solutions found, even when some of them could be undesirable or impractical in a mechanical device.

4.1. Geometric conditions

Once the end-effector is located at a certain desired pose (IK inputs), coordinates of the hinged joint B_i of each leg are known, as well as the fixed locations of sliding guides or revolute or prismatic input joints. These conditions were enough for getting a feasible solution in the case of rigid links parallel mechanisms, but not in flexible ones.

For leg type $\underline{P}FR$, see Fig. 5(a), as B_i location is given, the flexible rod can be deformed into many different shapes corresponding to different input values ρ_i, and different forces and deformation energy values. They will correspond to an infinite subset of the $k^i - \psi^i$ space of all possible deformations of the rod. Conversely, in the rod's local frame $(\mathcal{A}_i,\ x_i y_i)$ such geometric condition corresponds to all possible deformed shapes of the rod with a fixed A_i extreme and a given value of B_i end-tip's y coordinate, i.e. $y_i = h$, as shown in Fig. 5(b).

As the space of all deformed solutions of a rod $k^i - \psi^i$ can be represented by Fig. 2(a), those fulfilling the above-mentioned condition will be a subset of $k^i - \psi^i$ for a chosen d-mode q, so that Eq. (13) particularized with Eq. (11) equals h. Those duples in the subset correspond to different end-tip forces at B_i, and they should be checked for overall equilibrium later on. Note that IK solutions provide actuators' values ρ_i, which are derived from the local x_i coordinate of the end-tip and the given coordinates of points B_i.

Finding the subset $k^i - \psi^i$ is developed further on here. As explained in Section 2, elliptic integrals functions provide an analytical integration of Kirchhoff model equations, each deformed shape depending on parameters k and ψ defined in closed ranges $[-1, 1]$ and $[0, 2\pi]$ respectively. However, boundary conditions of the rod at extremes reduce this space further, for example for clamped-hinged rods Eq. (10) applies and a minimum value of k is required, depending on ψ, to get a real number. Hence, as shown in Fig. 6(a), the values of k^i are in the restricted ranges $\left[-1, -k^i_{min}\right]$ and $\left[k^i_{min}, 1\right]$.

To sample values of k^i and ψ^i such that a variation in the conditions is evenly represented, a transformation of parameter k^i is proposed as k^i_r, providing a rectangular range as shown in Fig. 6(b):

$$k^i_r = sign(k^i) \cdot \frac{|k^i| - |k^i_{min}|}{1 - |k^i_{min}|} \tag{14}$$

Moreover, grid density for sampling can be adjusted with a higher density in areas where we observe that the results change rapidly.

Then, applying the geometric condition defined before, we get a subset of $k^i_r - \psi^i$ that can be represented with the curves shown in Fig. 7.

In the case of a $\underline{R}FR$ leg type (see Fig. 8(a)), for given IK location of B_i and being A_i fixed, all possible deformed shapes for rod i are those with a known distance $A_i - Bi$ between end-tips. Conversely, in the local frame, they will be those whose end-tips are located on a circumference of radius r (see Fig. 8(b)). The corresponding subset of $k^i - \psi^i$ can be found as before, imposing the condition $x^2 + y^2 = r^2$ with Eqs. (12) and (13) particularized with Eq. (11).

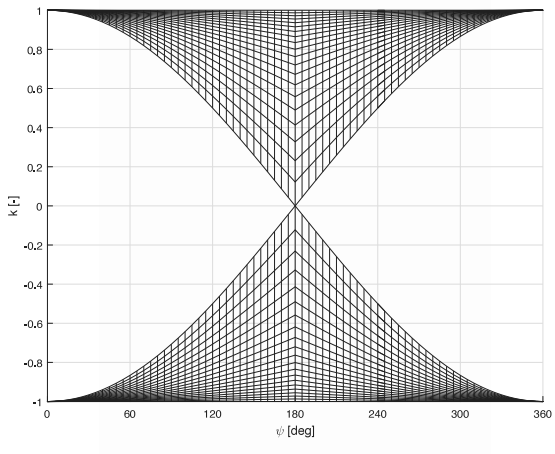

(a) Space $k^i - \psi^i$

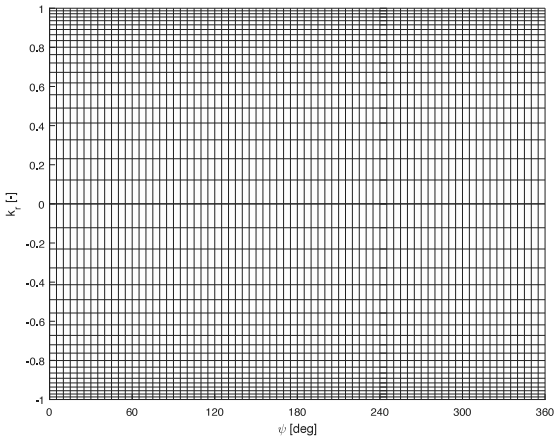

(b) Space $k_r^i - \psi^i$

Fig. 6. Comparison of Parameter Spaces alternatives.

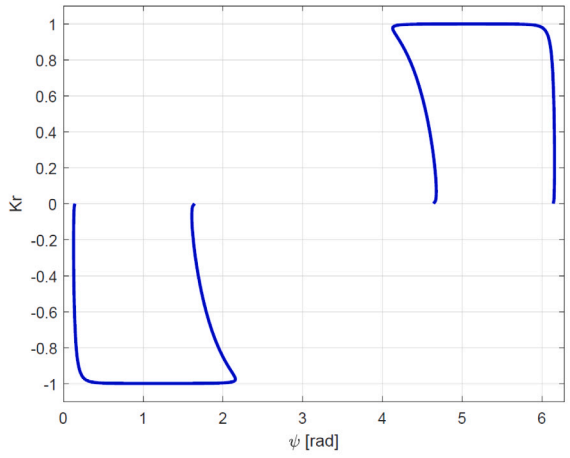

Fig. 7. Curves in $k_r^i - \psi^i$ verifying the geometric condition.

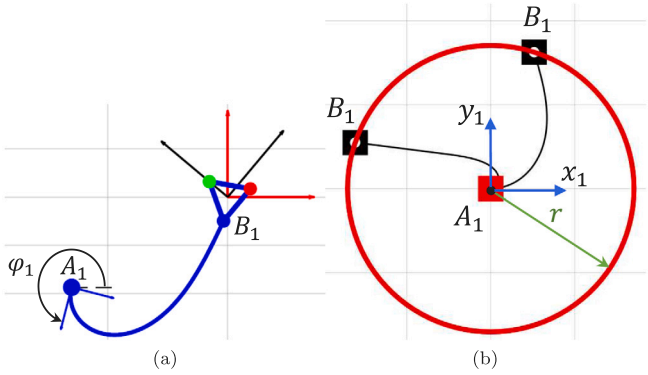

Fig. 8. Geometric condition for leg type $\underline{R}FR$.

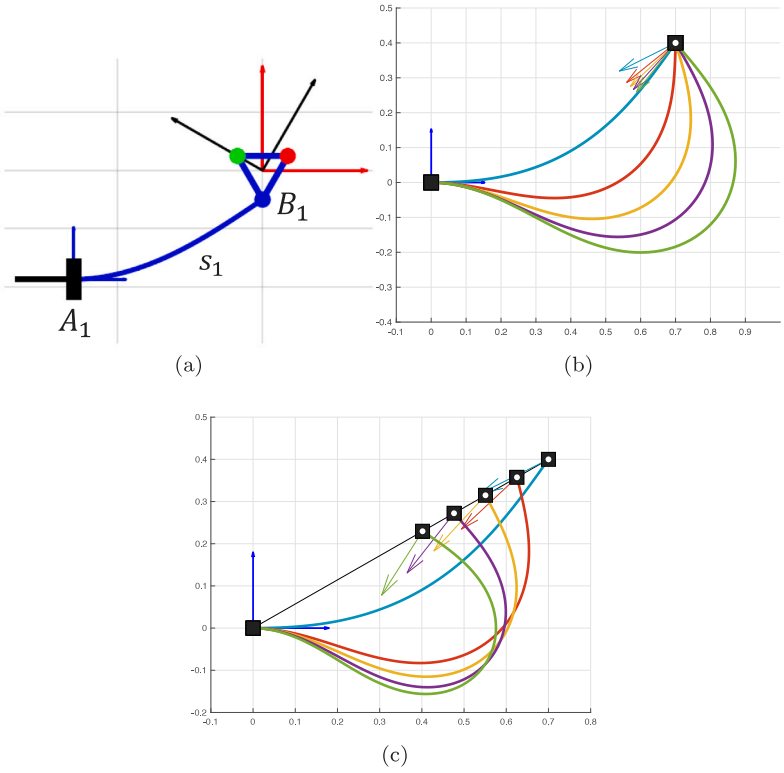

Fig. 9. Geometric condition for leg type $P\underline{F}R$.

Finally, for leg type $P\underline{F}R$ (see Fig. 9(a)), the subset of solutions will be those deformed shapes of rod with variable flexible leg lengths s_i that place end-tips A_i and B_i on fixed given locations as shown in Fig. 9(b). The geometric condition used is somewhat different than in previous cases, where rod's length was constant and known L. We need to use a unit length rod and the local frame to define the general geometric condition for the IK problem, whereas the actual rods' lengths will the final solution. For that purpose, we follow this rationale: those potential solutions under the IK geometric requirement shown in Fig. 9(b), when linearly scaled to a rod's unit length become into the rods' shapes shown in Fig. 9(c). Hence, the geometric condition for unit length rod can be stated as that end-tip of rod should be located on the line of known direction defined by A_i and B_i, i.e. a line at a constant angle β, as shown in Fig. 9(c). The corresponding subset of $k^i - \psi^i$ can be found as above, imposing the condition $y/x = \tan\beta$ with Eqs. (12) and (13) particularized with Eq. (11). Then, all those solutions are scaled to the actual locations of A_i and B_i.

4.2. Static equilibrium

The following step is to find which of the different combinations of possible deformed shapes of rods given by the three subsets of $k^i - \psi^i$ (as those in Fig. 7) generate a static equilibrium of forces and moments at the end effector, including not only the end-forces R^i due to the deformation of the rods, but the load wrench, i.e., F_X, F_Y, and M_Z. In the global fixed frame, using the corresponding rotation matrices for each rods' local frame $\mathbf{R}_i^F$ that may depend on the inputs, and taking moments about the loading point on the end effector, we get:

$$\begin{aligned} &\sum_{i=1}^{3} \mathbf{R}_i^F \cdot \begin{Bmatrix} R^i \cos\psi^i \\ R^i \sin\psi^i \end{Bmatrix} + \begin{Bmatrix} F_X \\ F_Y \end{Bmatrix} = \begin{Bmatrix} 0 \\ 0 \end{Bmatrix} \\ &\sum_{i=1}^{3} \mathbf{b}^i \times \mathbf{R}_i^F \cdot \begin{Bmatrix} R^i \cos\psi^i \\ R^i \sin\psi^i \end{Bmatrix} + M_Z \mathbf{k} = \mathbf{0} \end{aligned} \tag{15}$$

where $\mathbf{b}^i$ is the location of the end-point attachments on the end effector B_i with respect to the loading point P.

In order to find all solutions, certified methods as [21] can be used to get $k^i - \psi^i$ final solutions. Also, global minimization processes on Eq. (15) from previous subsets $k^i - \psi^i$ generate the multiple solutions of the IK problem with no formal guarantee of certified complete solution. In the latter case, depending on the numerical sampling, approximate solutions are found, and a refinement procedure is advised. In such case, it is convenient to apply direct numerical integration on Eqs. (5) and (7), and a Newton scheme to geometric and static constraints to refine those approximate solutions. Finally, if a more realistic model is required for the material properties or nonlinear deformations, the obtained solutions of the Kirchhoff model can be used as starting guess poses to be optimized on the improved model.

4.3. Stability of equilibrium

A configuration on equilibrium of the flexible mechanism is reached when the potential energy of the mechanical system is on a stationary state. This can correspond to a local minima of the energy function which means that an stable equilibrium configuration is reached, or any other situations that mean an unstable equilibrium (usually saddle points of the energy function [23]). Unstable equilibria are hardly reached in practice because the system moves out of it under any small perturbation, and therefore are solutions of the position problem that must be discarded in the procedure. Such instabilities of the flexible mechanism can occur at any point of the rods in the system [25]. Therefore, a variational approach should be considered for a comprehensive analysis of this phenomenon. In the procedure proposed here, we have included the instability analysis of the aforementioned mechanisms following the seminal work in [16], and adding to the line of calculus presented in [23]. If the analysis performed indicates that the static equilibrium obtained is unstable, it is discarded as a plausible solution.

4.4. Kinematic Jacobians and singularities

Once the procedure has provided the multiple stable solutions for the IK problem, these need to be evaluated regarding kinematic properties and singularities, which requires finding the Kinematic Jacobian matrices. In rigid-link parallel manipulators, as the Jacobian is defined analytically, we can obtain the geometric conditions for singular poses, which eventually leads to the finding of singularity locus. However, this is not the case in continuum parallel manipulators, because the Jacobians are numerically obtained at each pose by applying an iterative position analysis with small displacements around the studied pose of either inputs $\Delta\boldsymbol{\rho}$ or outputs $\Delta\mathbf{x}_P$:

$$\begin{aligned} \Delta\mathbf{x}_P = \begin{Bmatrix} \Delta\mathbf{p}_P \\ \Delta\theta_P \end{Bmatrix} &= \mathbf{J}_{IK} \cdot \Delta\boldsymbol{\rho} \\ \Delta\boldsymbol{\rho} &= \mathbf{J}_{FK} \cdot \Delta\mathbf{x}_P \end{aligned} \tag{16}$$

Based on such approach, Jacobians can be evaluated and velocity ellipsoids found [23]. Singularities are here determined by proximity to singular conditions of Jacobians, which requires the evaluation of the position problem along a finite path or area so that relative values of the norms can be appropriately assessed to establish the singularity threshold, or, better, detecting changes of the sign of the norm of Jacobians on those paths. An in-depth singularity analysis is presented in [26], allowing a much more detailed classification of the singularities found.

4.5. Case studies

The Full IK solution procedure described has been applied to those flexible mechanisms declared in Section 3 with symmetric arrangements and simple regular dimensions so that analogies between the flexible manipulators under study and their rigid counterparts are easily appreciated. In subsequent figures, the different IK solutions found for a given output pose for each flexible manipulator will be shown. Bearing in mind that each leg can be working in a different d-mode, the set of solutions combining d-modes 1 and 2 will be represented. No higher d-modes have been tried because the deformation energy needed is much more higher, instabilities are therefore more prompt, and self-collisions of deformed rods are very common in such modes. No material limit has been considered so far, but that is another important issue preventing the possibility of having higher d-modes than two.

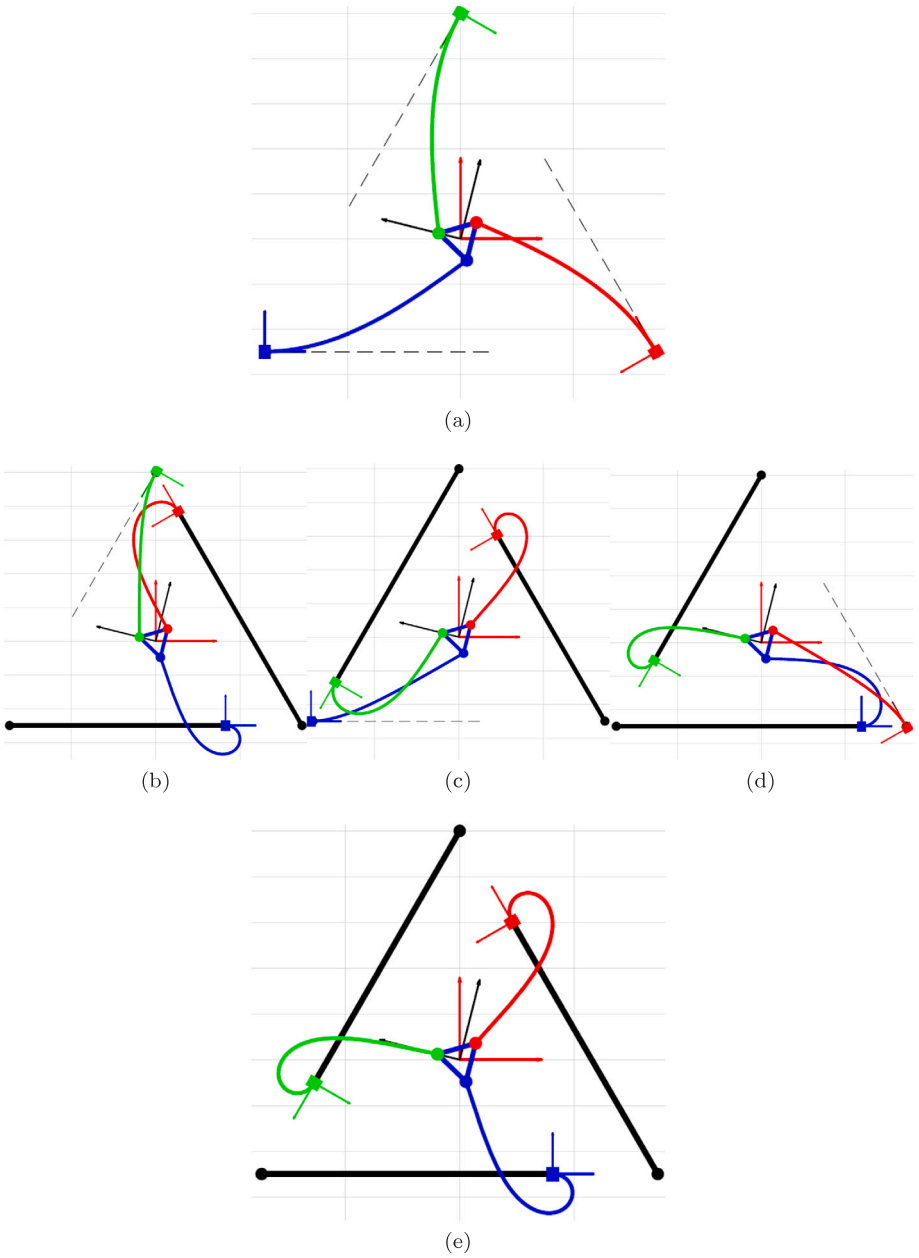

Fig. 10. PCM $3\underline{P}FR$: five IK solutions for mode 111 (1st d-mode in each leg).

In relation to PCM $3\underline{P}FR$, a set of possible IK stable solutions are represented in Figs. 10–12. In Fig. 10, the five IK solutions associated with mode 111, that is, d-mode 1 for each leg, are shown. In Fig. 11, the two IK solutions associated with mode 222, i.e. each leg in mode 2, are shown. Finally, in Fig. 12, one IK solution arises for the combination of modes 122, 212 and 221, respectively. Here it can be observed that deformation shapes with self collision loops appear in those rods with mode 2. Such occurrence can be also detected with geometric computation disregarding those IK solutions in an additional check.

Regarding the $3\underline{R}FR$, the set of possible IK solutions is represented in Fig. 13. In this case, eight solutions arise, all of them for mode 111, meaning that each leg is working in d-mode 1. The equivalent rigid manipulator, the $3\underline{R}RR$ (Fig. 4(b)), also has eight solutions of the IK problem. This can be the most appropriate example to appraise the similarities between rigid and flexible mechanisms.

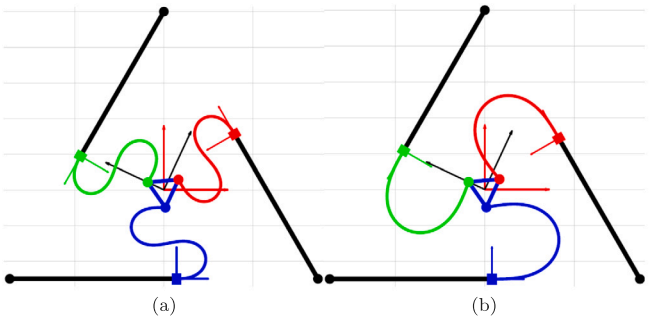

Fig. 11. PCM $3\underline{P}FR$: two IK solutions for mode 222 (2nd buckling mode in each leg).

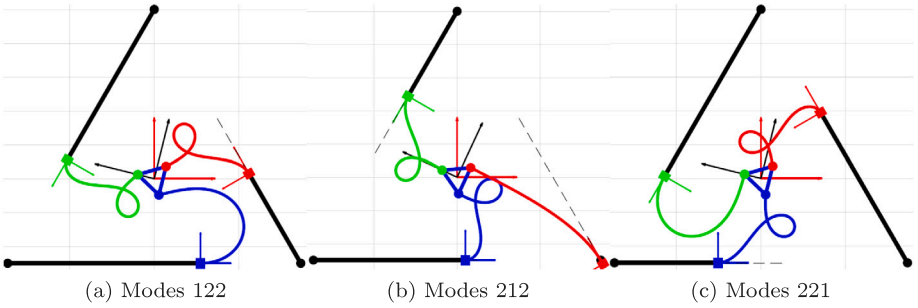

Fig. 12. PCM $3\underline{P}FR$: IK solutions for mixed modes.

Finally, in relation to PCM $3P\underline{F}R$, the set of possible IK solutions are represented in Figs. 14 and 15. In Fig. 14, the solutions for modes 111 and 222 can be seen, having one solution for mode 111 and two for mode 222. In the case of combining the d-modes in each leg, Fig. 15 shows the existence of one solution for each combination mode 122, 212 and 221.

5. Solving the full forward kinematic problem

The full FK problem has the objective of finding all possible poses of the end-effector for given values of the inputs at the motors and the load to be sustained. For all above-mentioned types of mechanisms, the actuation input condition means that first extreme of flexible rods A_i is given as well as its slope, i.e. the local frame i location is defined; and rods' lengths are known.

Solving the FK problem consist in finding the six parameters $k^i - \psi^i$ that define the deformed shape of flexible rods i of the mechanism, and eventually the pose of the end-effector given by position of their end-tips B_i. Two conditions must be fulfilled: that the end-tips assemble at the end-effector, and that forces imposed by those end-tips due to the rods' deformation on the end-effector produce a force equilibrium with the specified load.

First condition means, for a rigid-body triangular platform, that the three end-points B_i must fulfil rigid-body equations, i.e. that distances d_{ij} between the attachment points B_i and B_j, and angles β_{ijk} between sides B_iB_j and B_jB_k are constant. A sufficient condition being for example a choice of: distance d_{12} between B_1 and B_2, distance d_{13} between B_1 and B_3, and angle β_{213} between sides B_1B_2 and B_1B_3:

$$\begin{aligned} |\mathbf{p}^1(L_1) - \mathbf{p}^2(L_2)| &= d_{12} \\ |\mathbf{p}^1(L_1) - \mathbf{p}^3(L_3)| &= d_{13} \\ |\left(\mathbf{p}^1(L_1) - \mathbf{p}^2(L_2)\right) \times \left(\mathbf{p}^1(L_1) - \mathbf{p}^3(L_3)\right)| &= d_{12}d_{13}\sin\beta_{213} \end{aligned} \tag{17}$$

where $\mathbf{p}^i$ are coordinates of B_i in the fixed frame, and L_i are known rods' lengths. Second condition is that a static equilibrium is generated, as explained in Section 4.2, being expressed in Eq. (15).

The FK solving procedure starts with the definition of the sampling grid of parameters k^i and ψ^i as in Fig. 6, and the choice of the d-modes that will be searched. Then, a global optimization process is used with these 6 parameters (k^i and ψ^i) defined in closed ranges, and the 6 equations in Eqs. (15) and (17). As a result, we may get several 3-duples of parameters that provide the multiple FK solutions with that choice of d-modes. Those solutions are then checked for stability and singularity, providing the definite FK solutions. To complete the process, other possible combinations of d-modes at will are evaluated. As an example, the FK problem is solved for the $3\underline{R}FR$ flexible manipulator, considering combination mode 111. In this case, four stable solutions arise, these being represented in Fig. 16.

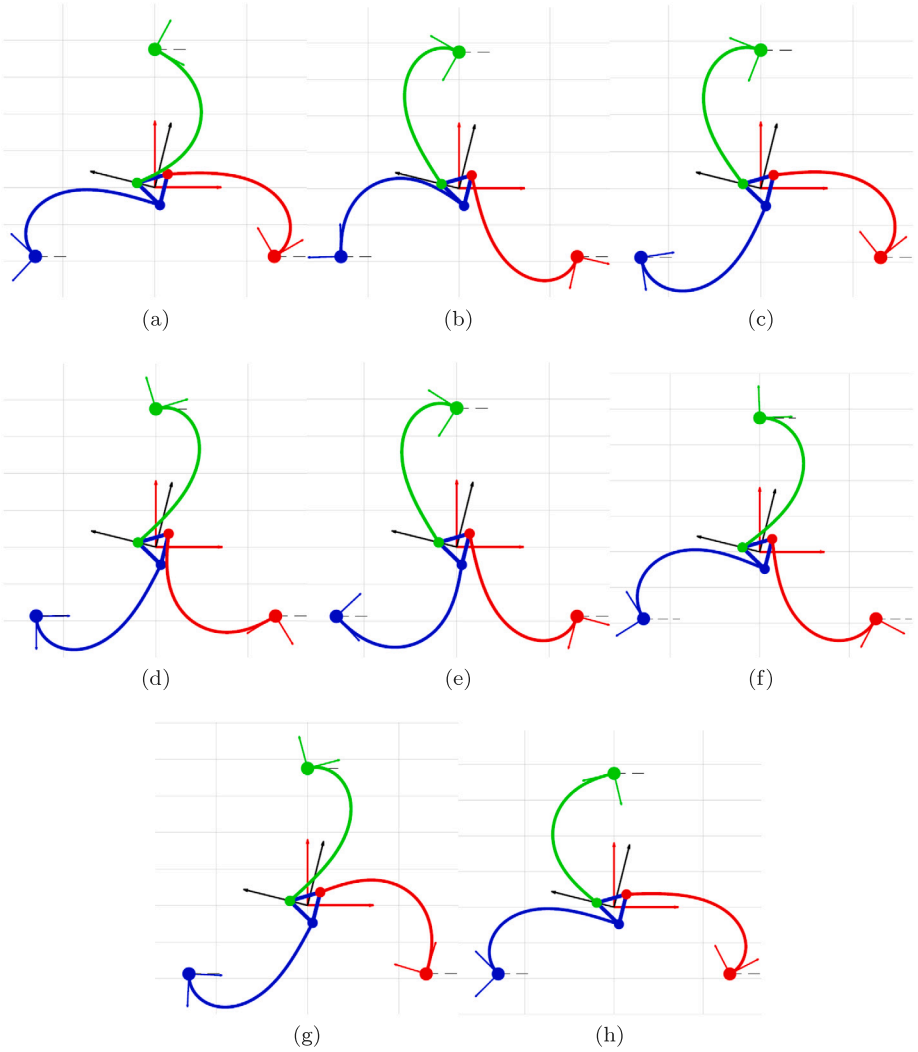

Fig. 13. PCM $3\underline{R}FR$: eight IK solutions for mode 111.

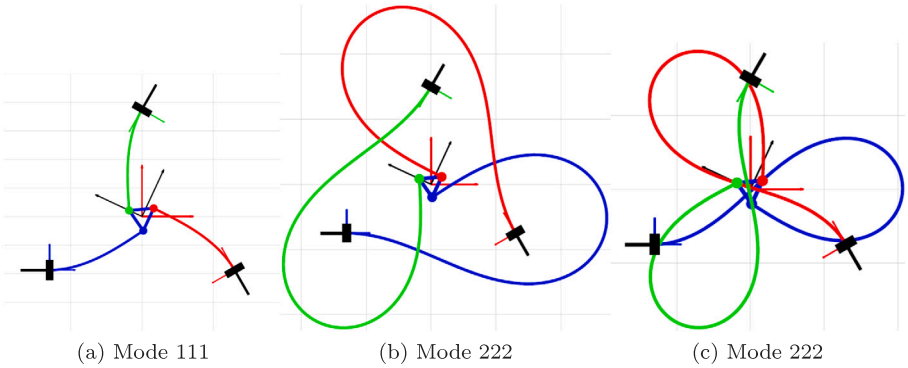

Fig. 14. PCM $3P\underline{F}R$ IK solutions. (For interpretation of the references to colour in this figure legend, the reader is referred to the web version of this article.)

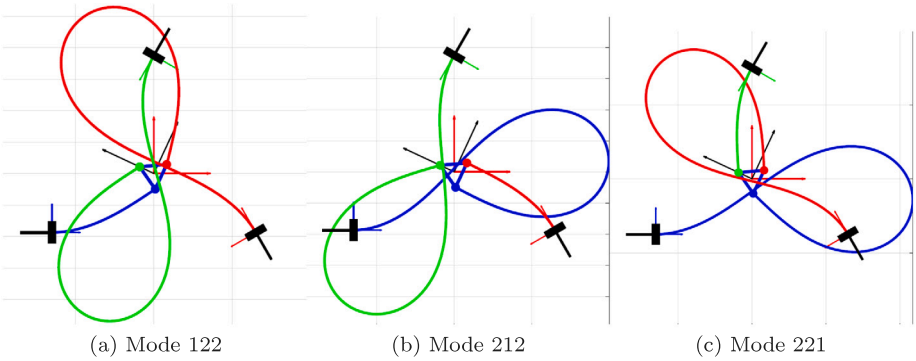

Fig. 15. PCM $3P\underline{F}R$: IK solution for mixed modes.

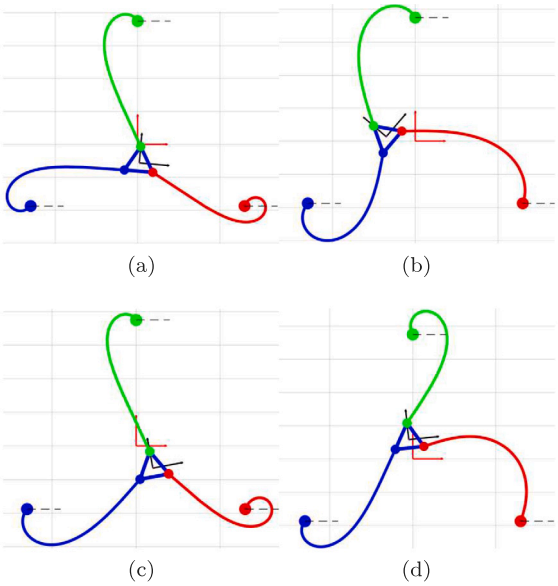

Fig. 16. Four FK solutions of the $3\underline{R}FR$: mode 111.

6. Workspace analysis

Workspace Analysis in the design stage consists in finding all reachable poses of a mechanism considering all possible assembly modes of the system. Each of the reachable singularity-free volumes are called aspects in classic rigid-link parallel kinematics. Those aspects can then be evaluated pose by pose to get kinematic performance indices to asses manipulability or to do an optimal design, being this still a controversial issue in Kinematics [27]. For Parallel Continuum manipulator the approach chosen is the analogous one. First, upon a choice of output pose and load, find the multiple stable solutions of the IK problem for the set of plausible buckling modes. Then, use each of them to start a numerical evaluation of the surrounding poses making use of the values of the state parameters obtained in the closest predetermined pose. Checking that the new obtained poses are continuous to the previous ones we can obtain each aspect, which requires evaluating Kinematic Jacobians to detect singularity boundaries.

In planar three degrees of freedom mechanisms, being the output pose variables X_p, Y_p, θ_p, the common approach is the evaluation of constant orientation workspaces for a set of desired orientations θ_p. For each of these constant orientation workspaces, the iterative procedure starts from a given pose with the desired orientation at some coordinates X_p, Y_p. Then, a wave propagation is initiated emanating from that position by step increments of those coordinates [28]. A direct numerical integration of the mechanism ODEs equations as in [14] is very efficient for this purpose, provided that the reference state parameters values are not far from the solution, which can be enforced by choosing a sufficient small step size. When no solution is reached, a boundary of the workspace corresponding to an IK singularity has been detected, being this verified by keeping a track of the evolution of the IK Jacobian norm. Upon evaluation of FK Jacobian, FK singularities are also detected, but are most efficiently found upon evaluation of instability which occurs simultaneously [23]. Wave propagation is stopped in the direction of singularity encounters.

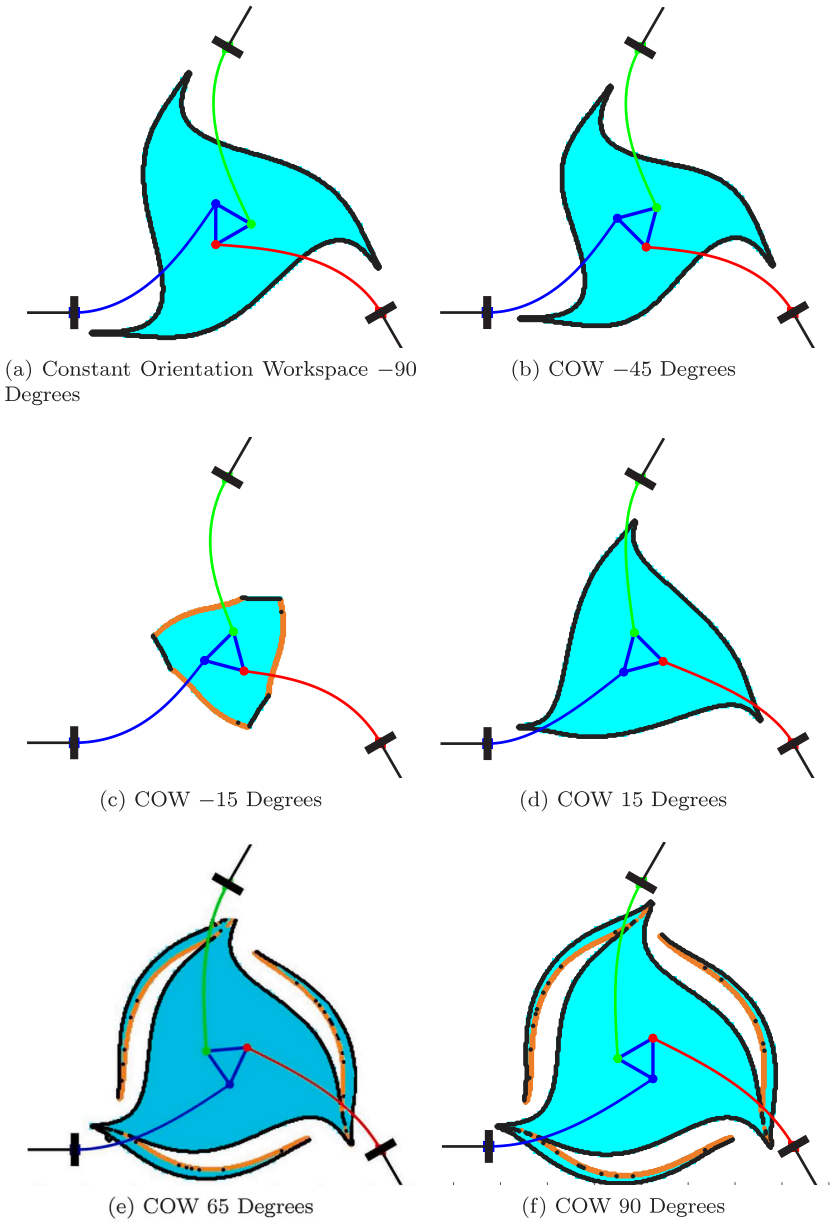

Fig. 17. One Aspect of the Workspace of the $3P\underline{F}R$ with initial modes 111.

As an example, different constant orientation workspaces are shown in Fig. 17 for the unique solution obtained of the $3P\underline{F}R$ with the mode combination 111 (as shown in Fig. 14(a)). IK singularities curves (depicted in black colour) can be found at the boundary of the workspace, while FK singularities, in orange, appear as boundaries of the workspace with instability areas.

An important issue is that, once the iterative process starts from a given pose with a choice of d-mode combination, there are continuous transitions between solutions that may involve a change of d-mode in some rod. The change of d-mode of rods is not a singularity or any other type of problem, it is a natural transition in the deformation mode of the flexible mechanism.

7. Experimental verification

In this section some issues related to practical application of the method are discussed and verified via experiments. The method assumes some simplifications that require some verification, from the use of the Kirchhoff rod model itself, to the final results of the position analysis and stability of the multiple solutions. Two test benches have been devised for this purpose.

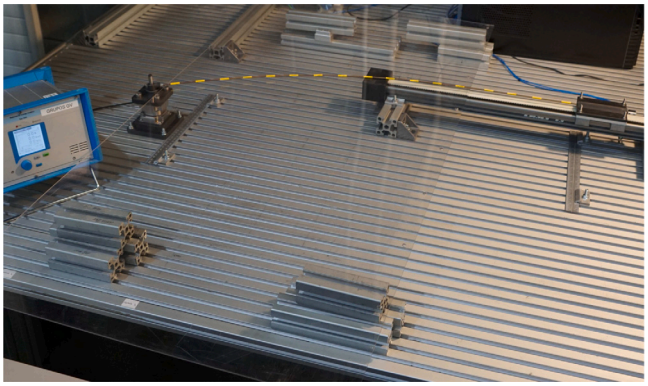

Fig. 18. Kirchhoff rod model testing.

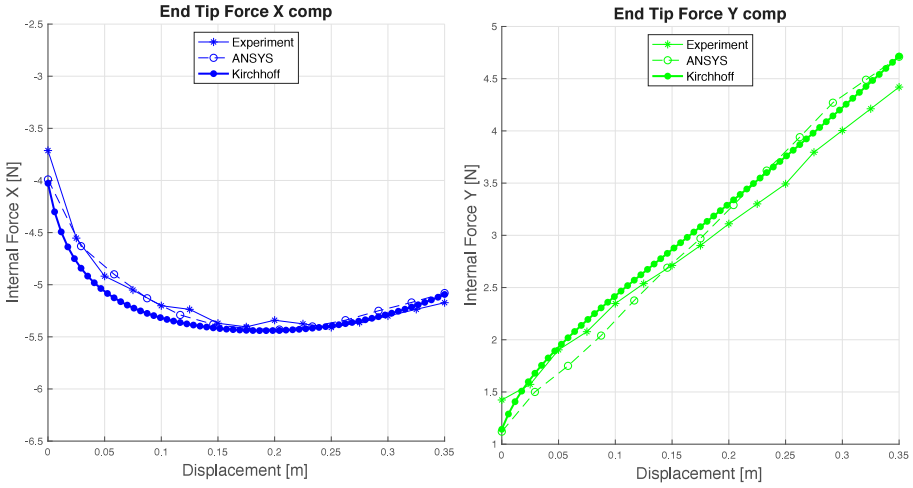

(a) X Component of End-tip Force (b) Y Component of End-tip Force

Fig. 19. Experimental Validation of Kirchhoff Model.

First, the Kirchhoff rod model is verified experimentally on the test arrangement shown in Fig. 18. A Nitinol elastic rod is tested, length of $L = 0.908$ [m] and a circular cross section of radius $r = 1.5$ [mm]. The material is modelled with a linear constitutive law whose Elastic modulus is $E = 68e^9$ [Pa] and Shear modulus $G = 25.5e^9$ [Pa]. The rod is pinned at its end-tip to a Kistler dynamometer where end-tip force components on a fixed cartesian frame are measured, while the other end is clamped to a linear actuator so that different bending configurations as in the geometric condition shown in Fig. 5(a) can be easily generated.

In order to justify the use of the Kirchhoff rod model, Eqs. (1)–(3) have to be considered. As the rod to be used has a Euler's critical load $P_{cri} = \pi^2 EI/(0.7L)^2 = 6.6$ [N], expected forces will be on the tenths of [N], and with values of $EA = 4.8e^5$ and $GA = 1.8e^5$ in Eqs. (2) and (3), the difference with respect to the Kirchhoff model values of $v_x = 1$ and $v_y = 0$ is of e^{-5} which justifies neglecting shear and extension effects.

Experimental results are obtained for a fixed y coordinate at the end-tip of -0.2125 [m] and a variable x coordinate going from 0.86 to 0.51 [m] as for Fig. 5(b). These experimental measurements are compared to those obtained with a nonlinear FEM analysis using ANSYS and the Kirchhoff rod model used in this paper, and are shown in Fig. 19. The differences are small enough to justify the simplification.

Once the elastic rod model has been verified, a second test bench is assembled to evaluate the effectiveness of the method to solve multiple solutions of a $3\underline{P}FR$ mechanism. As shown in Figs. 20, a $3\underline{P}FR$ mechanism is placed on a horizontal table where the end-effector has a reduced friction contact on the surface and it is unloaded. The dimensions chosen for the rods are the ones that verified the use of Kirchhoff model. These rods are clamped to linear actuators that are integrated in the system but the motion evaluated will be quasistatic. These linear guides are on the edges of a fixed equilateral triangle of circumcircle radius $r = 0.9$ [m]. Elastic rods are connected by revolute joints to the end-effector, that is an equilateral triangle with an edge length $a = 0.09$ [m].

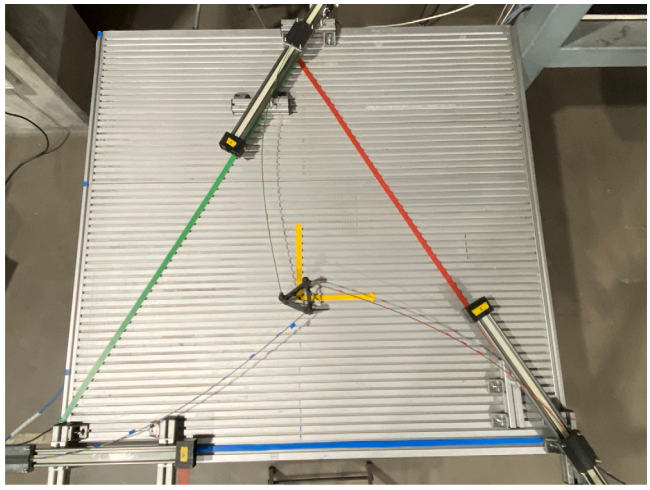

(a) FK solution 1

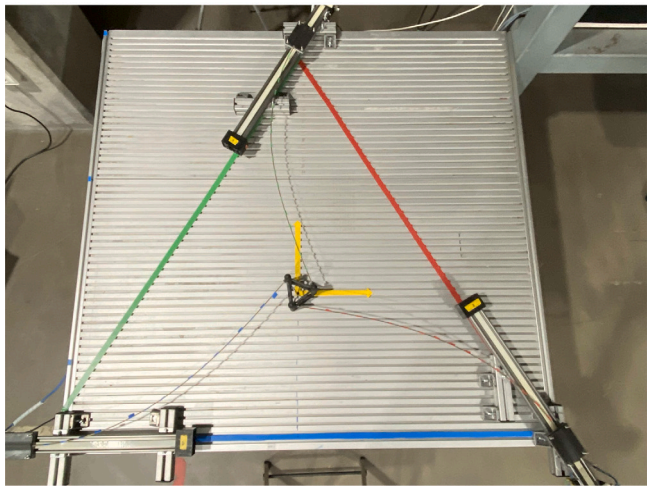

(b) FK solution 2

Fig. 20. Experimental Validation of $3\underline{P}FR$ mechanism.

Table 1
Theoretical and experimental results for the FK problem.

Outputs	FK solution 1		FK solution 2	
	Theory	Measured	Theory	Measured
x_P	0	−2 mm	0	8 mm
y_P	0	−2 mm	0	−1 mm
θ	90°	99°	−75.7°	−84°

First, a set of inputs is chosen and the multiple stable solutions of end-effector poses are measured to verify the accordance to solutions of the FK problem in Section 5. Input values are all equal to $\rho_i = 0.025$ [m], theoretical output poses and measured ones are presented in Table 1, and plot in Fig. 20.

Second, the input solutions found in the IK problem in Section 4 for given output poses are compared to the ones needed in the prototype to arrive to them. Several output poses with $x_P = y_P = 0$ and the following orientations $\theta = 60°, 90°, 120°$ are tested, with results given in Table 2.

These experimental results on prototypes with large dimensions and no calibration show a good agreement between the model and the actual mechanism behaviour. Nevertheless, if accuracy is important for the objective task a more complex model should be used as explained in the next section.

Table 2
Theoretical and experimental results for the IK problem.

Inputs	$\theta = 60°$		$\theta = 90°$		$\theta = 120°$	
	Theory	Measured	Theory	Measured	Theory	Measured
ρ_1 [m]	−0.007	−0.017	0.025	0.019	0.058	0.051
ρ_2 [m]	−0.007	−0.013	0.025	0.018	0.058	0.051
ρ_3 [m]	−0.007	−0.018	0.025	0.013	0.058	0.040

8. Conclusions

In this paper, we propose a procedure to solve the full position problem of planar parallel continuum mechanisms of three degrees of freedom with the following conditions: flexible elements are straight rods in free-stress reference configurations, no distributed forces or moments are considered to act along the length of the rod, a linear material constitutive law is used, and bending is the only source of deformation. A Kirchhoff model is used for the deformation, and a procedure is devised to take advantage of the special properties of the elliptic integrals functions that result in the integration of the nonlinear system of differential equations. The number of solutions obtained in the position problems is multiple, as it is commonly the case in their rigid-link counterparts, but the variability of the d-mode of the slender rods adds additional solutions. Deformation modes are important in contributing to such multiplicity, and must be addressed through the use of a suitable model, in this case, the elliptic integral solution method.

The procedure relies heavily in numerical routines subjected to tolerance thresholds that can burden the computational cost or lose some solution. To alleviate the first drawback, the procedure can be used with tolerance values that produce preliminary solutions with a limited accuracy, that is further improved using a direct integration approach [14] in a second stage.

The mechanisms chosen have rods connected to the end-effector via revolute joints, but a rigid connection could be also used. In such a case, the method should be adjusted to the new boundary condition with a change of ϕ_2 in Eq. (11), a change of the boundary conditions at B_i for the three mechanisms considered, and including the end-tip bending moments in the balance of moments in Eq. (15)

Also, if the deformation model is more complex, because other modes of deformation as shear or extension are relevant, or because a more complex material law is required, a Cosserat model should be used. Bear in mind that common superelastic materials have material laws that diverge from a linear elastic behaviour characterized by Young's Modulus E, in fact they may present an hysteretic behaviour, and that will affect the accuracy of results. The main problem to include such complex models is that such a model does not allow an easy integration resulting in elliptic integrals functions. We would like to emphasize that the focus of the paper is in the kinematic understanding of the performance of flexible parallel mechanisms that leads to the preliminary stages of design of such a device. The contribution is a method to solve the complete position analysis considering multiple solutions, stability issues, and eventually assembly modes and working modes of the mechanism that provide the best singularity free workspace. In order to be able to do that in a reasonable time, the price to pay is a simplification of the model so that elliptic integral approach can ensure a certified solution. Once the kinematician has chosen the mechanism for the task application, the next stage in the design will require a more detailed model to solve the position problem with the accuracy needed. That model will be a Cosserat model with the most appropriate material law, considering other effects than bending, and all distributed loads as own weight. Such a model will not be solvable with the elliptic integral approach and will require a direct integration of differential equations, but the results obtained with the proposed approach, by applying the Kirchhoff model, can be used as first approximations, that is, as initial guess, in a direct integration of those more complex models.

Declaration of competing interest

The authors declare that they have no known competing financial interests or personal relationships that could have appeared to influence the work reported in this paper.

Data availability

No data was used for the research described in the article.

Acknowledgements

The authors wish to acknowledge the financial support received from the Spanish Government through the Ministerio de Ciencia e Innovación (Project PID2020-116176GB-I00) financed by MCIN/AEI/ 10.13039/501100011033 and the support for the research group through Project IT1480-22 provided by the Departamento de Educación from the Regional Basque Government, Spain. Also, we want to express our gratitude to Javier Corral for his help with the ANSYS nonlinear analysis, and Luigi Tagliavini for his work in the prototype assembly.

References

[1] C.E. Bryson, D.C. Rucker, Toward parallel continuum manipulators, in: 2014 IEEE International Conference on Robotics and Automation, ICRA, 2014, pp. 778–785, http://dx.doi.org/10.1109/ICRA.2014.6906943.

[2] P.L. Anderson, A.W. Mahoney, R.J. Webster, Continuum reconfigurable parallel robots for surgery: Shape sensing and state estimation with uncertainty, IEEE Robot. Autom. Lett. 2 (3) (2017) 1617–1624, http://dx.doi.org/10.1109/LRA.2017.2678606.

[3] J. Burgner-Kahrs, D.C. Rucker, H. Choset, Continuum robots for medical applications: A survey, IEEE Trans. Robot. 31 (6) (2015) 1261–1280, http://dx.doi.org/10.1109/TRO.2015.2489500.

[4] L.L. Howell, Compliant Mechanisms, John Wiley and Sons, 2002.

[5] H. McClintock, F.Z. Temel, N. Doshi, J.-s. Koh, R.J. Wood, The milliDelta: A high-bandwidth, high-precision, millimeter-scale Delta robot, Science Robotics 3 (14) (2018) http://dx.doi.org/10.1126/scirobotics.aar3018.

[6] S.V. Levyakov, V.V. Kuznetsov, Stability analysis of planar equilibrium configurations of elastic rods subjected to end loads, Acta Mech. 211 (1) (2010) 73–87, http://dx.doi.org/10.1007/s00707-009-0213-0.

[7] S.M. Lyon, L.L. Howell, A simplified pseudo-rigid-body model for fixed-fixed flexible segments, in: Volume 5: 27th Biennial Mechanisms and Robotics Conference, 2002, http://dx.doi.org/10.1115/detc2002/mech-34203.

[8] G. Chen, Z. Zhang, H. Wang, A general approach to the large deflection problems of spatial flexible rods using principal axes decomposition of compliance matrices, J. Mech. Robot. 10 (3) (2018) http://dx.doi.org/10.1115/1.4039223.

[9] G. Chen, Y. Kang, Z. Liang, Z. Zhang, H. Wang, Kinetostatics modeling and analysis of parallel continuum manipulators, Mech. Mach. Theory 163 (2021) 104380, http://dx.doi.org/10.1016/j.mechmachtheory.2021.104380.

[10] X. Duan, W. Yan, G. Chen, H. Wang, Analysis and validation of a planar parallel continuum manipulator with variable Cartesian stiffness, Mech. Mach. Theory 177 (2022) 105030, http://dx.doi.org/10.1016/j.mechmachtheory.2022.105030.

[11] J.W. Wittwer, M.S. Baker, L.L. Howell, Simulation, measurement, and asymmetric buckling of thermal microactuators, Sensors Actuators A 128 (2) (2006) 395–401, http://dx.doi.org/10.1016/j.sna.2006.02.014.

[12] S.S. Antman, Nonlinear Problems of Elasticity, Springer, 2005.

[13] D.C. Rucker, R.J.W. III, Statics and dynamics of continuum robots with general tendon routing and external loading, IEEE Trans. Robot. 27 (6) (2011) 1033–1044, http://dx.doi.org/10.1109/TRO.2011.2160469.

[14] J. Till, C.E. Bryson, S. Chung, A. Orekhov, D.C. Rucker, Efficient computation of multiple coupled Cosserat rod models for real-time simulation and control of parallel continuum manipulators, in: Robotics and Automation (ICRA), 2015 IEEE International Conference on, IEEE, 2015, pp. 5067–5074, http://dx.doi.org/10.1109/ICRA.2015.7139904.

[15] A.L. Orekhov, V.A. Aloi, D.C. Rucker, Modeling parallel continuum robots with general intermediate constraints, in: 2017 IEEE International Conference on Robotics and Automation, ICRA, 2017, pp. 6142–6149, http://dx.doi.org/10.1109/ICRA.2017.7989728.

[16] J. Till, D.C. Rucker, Elastic stability of Cosserat rods and parallel continuum robots, IEEE Trans. Robot. 33 (3) (2017) 718–733, http://dx.doi.org/10.1109/TRO.2017.2664879.

[17] J. Till, D.C. Rucker, Elastic rod dynamics: Validation of a real-time implicit approach, in: 2017 IEEE/RSJ International Conference on Intelligent Robots and Systems, IROS, 2017, pp. 3013–3019, http://dx.doi.org/10.1109/IROS.2017.8206139.

[18] A.A. Alqumsan, S. Khoo, M. Norton, Robust control of continuum robots using Cosserat rod theory, Mech. Mach. Theory 131 (2019) 48–61, http://dx.doi.org/10.1016/j.mechmachtheory.2018.09.011.

[19] G. Gao, H. Wang, J. Liu, Y. Zheng, Statics analysis of an extensible continuum manipulator with large deflection, Mech. Mach. Theory 141 (2019) 245–266, http://dx.doi.org/10.1016/j.mechmachtheory.2019.07.015.

[20] O. Altuzarra, D. Caballero, F.J. Campa, C. Pinto, Position analysis in planar parallel continuum mechanisms, Mech. Mach. Theory 132 (2019) 13–29, http://dx.doi.org/10.1016/j.mechmachtheory.2018.10.014.

[21] O. Altuzarra, J.P. Merlet, Certified kinematics solution of 2-DOF planar parallel continuum mechanisms, in: T. Uhl (Ed.), Advances in Mechanism and Machine Science, Springer International Publishing, 2019, pp. 197–208, http://dx.doi.org/10.1007/978-3-030-20131-9_20.

[22] O. Altuzarra, D. Caballero, Q. Zhang, F.J. Campa, Kinematic characteristics of parallel continuum mechanisms, in: J. Lenarcic, V. Parenti-Castelli (Eds.), Advances in Robot Kinematics 2018, Springer International Publishing, 2019, pp. 293–301, http://dx.doi.org/10.1007/978-3-319-93188-3_34.

[23] O. Altuzarra, F.J. Campa, On singularity and instability in a planar parallel continuum mechanism, in: J. Lenarcic, B. Siciliano (Eds.), Advances in Robot Kinematics 2020, Springer International Publishing, 2021, pp. 327–334, http://dx.doi.org/10.1007/978-3-030-50975-0_40.

[24] A. Zhang, G. Chen, A comprehensive elliptic integral solution to the large deflection problems of thin beams in compliant mechanisms, J. Mech. Robot. 5 (2) (2013) 021006, http://dx.doi.org/10.1115/1.4023558.

[25] T. Bretl, Z. McCarthy, Quasi-static manipulation of a Kirchhoff elastic rod based on a geometric analysis of equilibrium configurations, Int. J. Robot. Res. 33 (1) (2014) 48–68, http://dx.doi.org/10.1177/0278364912473169.

[26] S. Briot, A. Goldsztejn, Singularity conditions for continuum parallel robots, IEEE Trans. Robot. 38 (1) (2022) 507–525, http://dx.doi.org/10.1109/TRO.2021.3076830.

[27] J.-P. Merlet, Parallel robots: Open problems, in: J.M. Hollerbach, D.E. Koditschek (Eds.), Robotics Research, Springer London, London, 2000, pp. 27–32, http://dx.doi.org/10.1007/978-1-4471-0765-1_4.

[28] E. Macho, O. Altuzarra, C. Pinto, A. Hernandez, Workspaces associated to assembly modes of the 5R planar parallel manipulator, Robotica 26 (3) (2008) 395–403, http://dx.doi.org/10.1017/S0263574707004109.